

---

This is an electronic reprint of the original article.  
This reprint may differ from the original in pagination and typographic detail.

Wong, William S.Y.; Kiseleva, Mariia S.; Zhou, Shaochen; Junaid, Muhammad; Pitkänen, Leena; Ras, Robin H.A.

## Design of Fluoro-Free Surfaces Super-Repellent to Low-Surface-Tension Liquids

*Published in:*  
Advanced Materials

*DOI:*  
[10.1002/adma.202300306](https://doi.org/10.1002/adma.202300306)

Published: 20/07/2023

*Document Version*  
Publisher's PDF, also known as Version of record

*Published under the following license:*  
CC BY

*Please cite the original version:*  
Wong, W. S. Y., Kiseleva, M. S., Zhou, S., Junaid, M., Pitkänen, L., & Ras, R. H. A. (2023). Design of Fluoro-Free Surfaces Super-Repellent to Low-Surface-Tension Liquids. *Advanced Materials*, 35(29), Article 2300306 .  
<https://doi.org/10.1002/adma.202300306>

---

This material is protected by copyright and other intellectual property rights, and duplication or sale of all or part of any of the repository collections is not permitted, except that material may be duplicated by you for your research use or educational purposes in electronic or print form. You must obtain permission for any other use. Electronic or print copies may not be offered, whether for sale or otherwise to anyone who is not an authorised user.

# Design of Fluoro-Free Surfaces Super-Repellent to Low-Surface-Tension Liquids

William S. Y. Wong,\* Mariia S. Kiseleva, Shaochen Zhou, Muhammad Junaid, Leena Pitkänen, and Robin H. A. Ras\*

Super-liquid-repellent surfaces feature high liquid contact angles and low sliding angles find key applications in anti-fouling and self-cleaning. While repellency for water is easily achieved with hydrocarbon functionalities, repellency for many low-surface-tension liquids (down to  $30 \text{ mN m}^{-1}$ ) still requires perfluoroalkyls (a persistent environmental pollutant and bioaccumulation hazard). Here, the scalable room-temperature synthesis of stochastic nanoparticle surfaces with fluoro-free moieties is investigated. Silicone (dimethyl and monomethyl) and hydrocarbon surface chemistries are benchmarked against perfluoroalkyls, assessed using model low-surface-tension liquids (ethanol–water mixtures). It is discovered that both hydrocarbon- and dimethyl-silicone-based functionalization can achieve super-liquid-repellency down to  $40\text{--}41 \text{ mN m}^{-1}$  and  $32\text{--}33 \text{ mN m}^{-1}$ , respectively (vs  $27\text{--}32 \text{ mN m}^{-1}$  for perfluoroalkyls). The dimethyl silicone variant demonstrates superior fluoro-free liquid repellency likely due to its denser dimethyl molecular configuration. It is shown that perfluoroalkyls are not necessary for many real-world scenarios requiring super-liquid-repellency. Effective super-repellency of different surface chemistries against different liquids can be adequately predicted using empirically verified phase diagrams. These findings encourage a liquid-centric design, i.e., tailoring surfaces for target liquid properties. Herein, key guidelines are provided for achieving functional yet sustainably designed super-liquid-repellency.

## 1. Introduction

Super-liquid-repellency,<sup>[1–7]</sup> from superhydrophobicity (water repellent)<sup>[3,4,8]</sup> to superomniphobicity (water and oil repellent),<sup>[1,2,9,10–13]</sup> is intensively studied from both fundamental and applied perspectives. This unique wetting phenomenon depends on two dominant contributing factors, namely, surface topography and surface chemistry. Investigations into the former have provided a detailed understanding of how re-entrant geometries<sup>[2,5,13–15]</sup> are vital toward the repellency of low-surface-tension liquids. Understanding of the optimal design/choice of surface chemistry, however, is comparatively scarce. This is further bracketed by the popularity of perfluoroalkyl chemistry, justified under the conceptual lowest known surface energy of a  $-\text{CF}_3$  group.<sup>[16]</sup> As a result, this culminates in the dominion of perfluoroalkyl chemistry within the state-of-the-art, regardless of any actual requirements in superhydrophobicity or superomniphobicity.<sup>[7,6,17,18]</sup>

Despite the well-demonstrated performance of perfluoroalkyls<sup>[17,19–24]</sup> in the domain of super-liquid-repellency, the continued use of perfluoroalkyl chemistry as a crude all-encompassing solution

brings long-term environmental and health hazards.<sup>[25–29]</sup> This is caused by the poor biodegradability and complex remediation (albeit progressing<sup>[30]</sup>) of perfluoroalkyls under ambient conditions (impervious to environmental UV light and/or temperature).<sup>[29]</sup> Today, the bioaccumulation of perfluoroalkyls is observed in both human blood and wildlife,<sup>[27]</sup> with epidemiological studies already correlating perfluoroalkyl exposure to carcinoma and heart diseases amongst other ailments.<sup>[25,28]</sup> Efforts to replace long-chain perfluoroalkyls (so-termed  $\text{C}_8$ ) with short-chain perfluoroalkyls<sup>[31]</sup> will bypass legislations (as of the time of writing) but will not avoid these hazards.<sup>[25]</sup> In Europe, an EU-wide perfluoroalkyl substances (PFAS) ban may be enacted as soon as 2025.<sup>[32]</sup>

Here, we discuss potential alternatives to perfluoroalkyl chemistry for super-liquid-repellency. A careful review of silicone or hydrocarbon chemistries (so-termed fluoro-free) suggests that both variants have yet to be exploited to their maximum potential in

W. S. Y. Wong, M. S. Kiseleva, S. Zhou, M. Junaid, R. H. A. Ras  
Department of Applied Physics  
School of Science  
Aalto University  
Espoo FI-02150, Finland  
E-mail: william.wong@aalto.fi; robin.ras@aalto.fi

L. Pitkänen  
Department of Bioproducts and Biosystems  
School of Chemical Engineering  
Aalto University  
Espoo FI-02150, Finland

 The ORCID identification number(s) for the author(s) of this article can be found under <https://doi.org/10.1002/adma.202300306>

© 2023 The Authors. Advanced Materials published by Wiley-VCH GmbH. This is an open access article under the terms of the Creative Commons Attribution License, which permits use, distribution and reproduction in any medium, provided the original work is properly cited.

DOI: 10.1002/adma.202300306

super-liquid-repellency (Table S1, Supporting Information). Very recent studies have employed silicones for oleophobic fabrics<sup>[34]</sup> and omniphobic surfaces,<sup>[34]</sup> but in contrast to the super-liquid-repellent state, these do not rapidly repel low-surface-tension liquids. In fact, most studies in super-liquid-repellency utilizing fluoro-free precursors are only tested against pure water, salt-water, or (at most) ethylene glycol with high surface tensions ( $\gamma \geq 72.8 \text{ mN m}^{-1}$ <sup>[35,36]</sup> or  $\gamma = 47.7 \text{ mN m}^{-1}$ <sup>[37–39]</sup>) to demonstrate simple superhydrophobicity (Table S2, Supporting Information). There remains a surprising lack of investigations into fluoro-free chemistries for low-surface-tension super-liquid-repellency.

Difluoromethylene ( $-\text{CF}_2$ ) and trifluoromethyl ( $-\text{CF}_3$ ) groups possess some of the lowest surface energies at  $\approx 19 \text{ mJ m}^{-2}$ <sup>[40]</sup> and  $\approx 6 \text{ mJ m}^{-2}$ <sup>[16]</sup> respectively. Perfluoroalkyls are typically composed of both functional groups, leading to a net surface energy of between  $11\text{--}19 \text{ mJ m}^{-2}$ .<sup>[41]</sup> In contrast to this, the methylene ( $-\text{CH}_2$ ) and methyl ( $-\text{CH}_3$ ) groups possess significantly higher surface energies of  $\approx 33 \text{ mJ m}^{-2}$ <sup>[40]</sup> and  $\approx 19\text{--}21 \text{ mJ m}^{-2}$ ,<sup>[41]</sup> respectively. Common hydrophobic polymers are composed primarily of methylene groups, leading to a surface energy of  $\approx 30 \text{ mJ m}^{-2}$ .<sup>[40]</sup> Curiously, the pure methyl ( $-\text{CH}_3$ ) functionality, of  $\approx 19\text{--}21 \text{ mJ m}^{-2}$ <sup>[41]</sup> may be easily achieved at scale via the route of dimethyl silicone chemistry, where two  $-\text{CH}_3$  groups are held by a siloxane backbone,  $[\text{O}-\text{Si}(\text{CH}_3)_2]_x$ . In this work, we show that carefully optimized silicone functionalization can match the liquid repellency of perfluoroalkyls under many real-world (aqueous-based) situations. The technique demonstrated employs simple green solvents,<sup>[42,43]</sup> is highly scalable, and processable at room temperature. We highlight the performance limits of silicone-, hydrocarbon-, and perfluoroalkyl- functionalization, alongside predictions made by empirically-verified repellency phase maps. We believe that the use of such phase maps can be used to guide fluoro-free surface chemistry designs, by focusing on target liquid properties. These design principles outline how future generations of fluoro-free super-liquid-repellent surfaces can be sustainably achieved.

## 2. Results and Discussion

### 2.1. Design: Liquid vs Vapor Functionalization of Fluoro-Free Nanoparticle-Based Surfaces

The silicone-based dimethyl ( $-\text{CH}_3$ )<sub>2</sub> surface functionalization is based on the dichlorodimethylsilane (DCDMS) precursor. DCDMS reacts through hydrolysis and condensation<sup>[34]</sup> to create siloxane backbone chains of  $-\text{Si}-\text{O}-\text{Si}-$  bearing dimethyl functionalities on each Si atom,  $\text{O}-\text{Si}(\text{CH}_3)_2$ . Due to the dichloro-bifunctionality, siloxane chains (silicones) are formed (Figure 1a). To achieve super-liquid-repellency, we introduce nanometric surface topographies<sup>[2,6,19,21,44]</sup> and explore two approaches (Figure 1b,c) for surface functionalization. In each separate instance (liquid- or vapor-functionalization), the use of identical nanoparticles as starting materials standardizes our investigation into surface chemistry variations. Four variants are examined: dimethyl silicone (DCDMS), monomethyl silicone (trichloromethylsilane, TCMS), hydrocarbon-functionalized (trichloro(octyl)silane, OTS), and perfluoroalkyl (perfluoro(octyl)silane, PFOTS).

In the first instance, a classic in-liquid functionalization technique<sup>[19,20,45,46]</sup> is employed. 1 g of fumed silica is mixed

into 30 mL of chloroform, followed by adding excess chlorosilanes, e.g. DCDMS at 6 times (0.86 mL) the theoretical hydroxyl concentration ( $4 \mu\text{mol per m}^2$ ).<sup>[47,48]</sup> Chloroform was chosen as the solvent of choice due to its excellent solvation properties<sup>[49]</sup> and track record for dense surface functionalization with chlorosilanes.<sup>[19,45]</sup> The reaction is allowed to proceed at  $20^\circ\text{C}$  for 72 h, before three cleaning cycles (chloroform washing) and collection (vacuum drying) of liquid-functionalized silica particles. Functionalized silica is then re-dispersed in acetone at  $10 \text{ mg mL}^{-1}$  and spray-coated ( $10 \text{ mL per } 37.5 \text{ cm}^2$ ) onto glass substrates at a working distance of 10 cm at a pressure of 3 bar (Figure 1b). The resulting surfaces are nano(micro)structured (Figure 1d,e, top and side view), with a mean particle size of  $55 \pm 11 \text{ nm}$ . Surfaces are free of fluoro-functionality (Figure 1e).

In the second instance, a classic in-(chemical)-vapor-functionalization (CVD, vapor-functionalization) technique is employed.<sup>[6,21]</sup> Plain, unfunctionalized fumed silica is dispersed in acetone at  $10 \text{ mg mL}^{-1}$  and spray-coated ( $10 \text{ mL per } 37.5 \text{ cm}^2$ ) onto glass substrates at a working distance of 10 cm at a pressure of 3 bar. Thereafter, surfaces are exposed to chlorosilanes, e.g. DCDMS in a desiccator (20 cm diameter,  $V = 4.2 \text{ L}$ ) at  $\approx 8 \text{ cm}$  from a central source (0.5 mL) at 50 mbar for 120 min (Figure 1c, optimized: Figure S2, Supporting Information). The resulting vapor-functionalized surfaces are also nano(micro)structured (Figure 1f,g, top and side view), with a notably coarser mean particle size of  $74 \pm 16 \text{ nm}$ . Differences in grain sizes and similarities in macroscopic roughness ( $R_q = 5\text{--}10 \mu\text{m}$ ) between vapor- and liquid-functionalization are also presented via transmission electron microscopy and optical profilometry (Figure S1, Supporting Information). Surfaces are free of fluoro-functionality (Figure 1g).

To assess surfaces for low-surface-tension liquid repellency, the use of ethanol–water mixtures is employed as a model liquid. This allows for tunable surface tension with both polar or non-polar (dispersive) components, per the weight percent of ethanol. The range (ethanol:water) goes from  $72.8 \text{ mN m}^{-1}$  (polar: dispersive at 2.3) to  $\approx 31\text{--}32 \text{ mN m}^{-1}$  (polar: dispersive at 0.48).

Static (CA) and sliding contact angle (SA) assessment ( $7 \mu\text{L}$  drops) vs net surface tension ( $\gamma$ ) show that both liquid- and vapor-functionalized surfaces are highly repellent ( $\text{CA} > 150^\circ$ ,  $\text{SA} < 10\text{--}15^\circ$ ) against pure water (Figure 1h,i,  $\gamma = 72.8 \text{ mN m}^{-1}$ ). However, complete wetting ( $\text{CA} = 0^\circ$ ) of the liquid-functionalized variant occurs at  $\gamma \approx 48\text{--}49 \text{ mN m}^{-1}$  (Figure 1h,i, red triangle). This behavior continues with increasing ethanol content (Figure 1h,i, red triangle at  $\gamma < 48.8 \text{ mN m}^{-1}$ ). In contrast, the vapor-functionalized variant shows a persistently high liquid repellency ( $\text{CA} > 150^\circ$ ,  $\text{SA} < 10^\circ$ ) down to  $\gamma \approx 32\text{--}33 \text{ mN m}^{-1}$  (Figure 1h,i, orange circle) before a mild wetting transition from between  $\gamma \approx 31\text{--}32 \text{ mN m}^{-1}$  (Figure 1h,i, orange circle) at a  $\text{CA} = 136^\circ$  and  $84^\circ$ ,  $\text{SA} \approx 12^\circ$  and pinned,  $90^\circ$  respectively.

The optimal nature of vapor-functionalization (for DCDMS) may be tentatively explained by molecular size. The dimethyl silicone precursor, DCDMS, is a much smaller molecule compared to commonly used  $\text{C}_6$  or  $\text{C}_8$  silanes (also discussed later). During liquid-functionalization, it is not sterically hindered and as a result, may form many unwanted and unanchored (i.e., solvated) silicone oligomers that are subsequently removed, thus reducing functionality. During vapor-functionalization, the small DCDMS

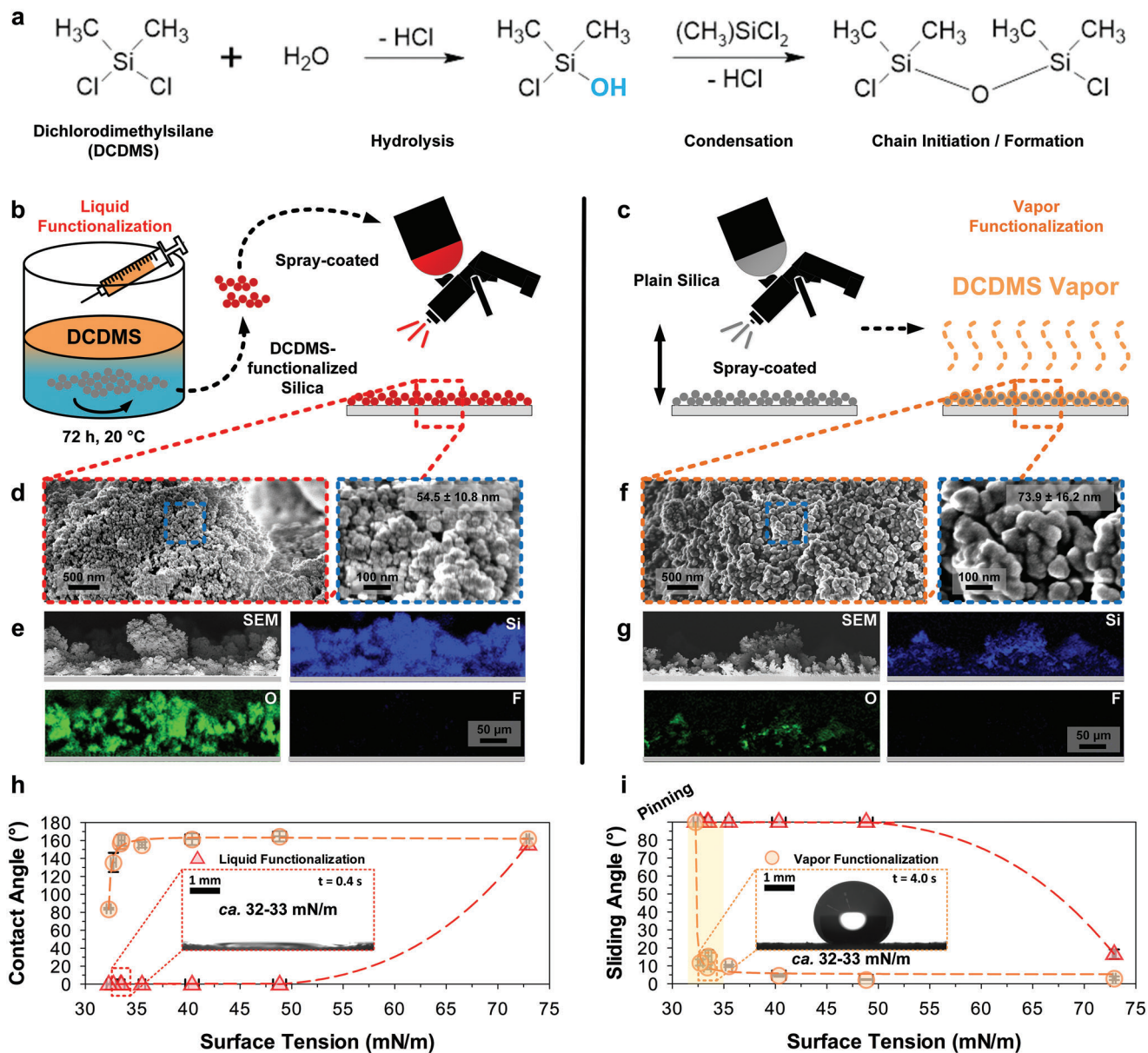


**Figure 1.** Conceptual design: functionalization of silicones using dichlorodimethylsilane (DCDMS) on silica nanoparticles. a) Bifunctionality of DCDMS forms purely dimethyl-functional siloxane chains after hydrolysis–condensation reactions. The schematized dimer will continue to react, forming chains. b) Approach #1. Liquid-functionalization by DCDMS leads to readily sprayable nanoparticulate coatings. c) Approach #2. Vapor-functionalization by DCDMS after spray-coating of plain nanosilica allows for denser surface functionalization. d–g) Nanoparticle surfaces are stochastically micro- and nanostructured. Elemental analysis shows the presence of Si, O but the absence of F. EDX spectra (cps/eV) are also provided in Figure S1 (Supporting Information). Vapor-functionalized nanoparticles appear to be larger during grain size analysis ( $74 \pm 16$  nm vs  $55 \pm 11$  nm). h,i) Wettability analysis ( $n = 3$ , mean  $\pm$  standard deviation) of contact angle (h) and sliding angle (i) shows drastic differences in performance between these two approaches for the super-liquid-repelling of low-surface-tension aqueous mixtures (model mixtures of ethanol–water). Experimental drop-on-surface images are included as insets within the dotted boxes (red: liquid-functionalized at 0.4 s, orange: vapor-functionalized at 4.0 s).

precursor easily vaporizes, forming dense vapor clouds that perform direct and continuous on-surface functionalization. Optionally, the framework of synthesis can also include an additional vapor-deposition (silica) step to improve stability, i.e., so-termed “stabilized” surfaces (see Supplementary Discussion, “Mechanical Stability Optimization” and Figure S3, Supporting Information). For conciseness and consistency, the following discussion will be based on the stabilized variant, unless otherwise indicated.

## 2.2. Mechanism: Silicone-on-Nanoparticle Growth (Self-Assembly)

To investigate the mechanism of silicone formation by DCDMS vapors on these nanostructured silica surfaces, high-resolution thin-film Fourier transform infrared (FTIR) spectroscopy is performed with respect to reaction time (Figure 2a,b). The reaction by vapor-functionalization occurs rapidly, within 5 min of

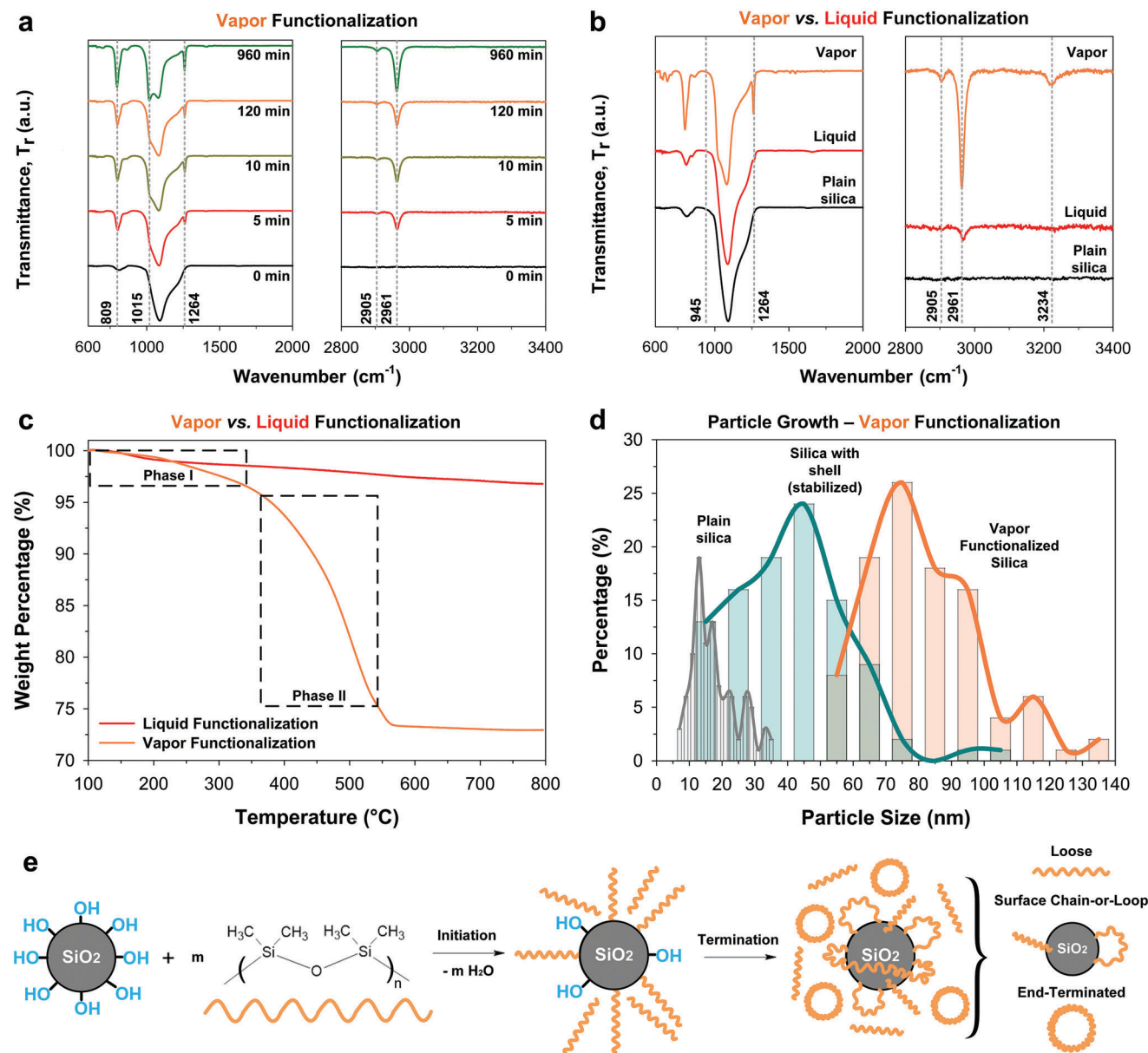


**Figure 2.** Mechanism: Spectroscopic, thermogravimetric, and growth mechanics of vapor-functionalization (dichlorodimethylsilane, DCDMS). a) Spectroscopic analysis from 0 min (plain silica “unstabilized”, black line) to 960 min of reaction time (functionalized silica, colored lines). Peak analysis:  $809 \text{ cm}^{-1}$  (rocking),  $1264 \text{ cm}^{-1}$  (symmetric deformation) of the Si–dimethyl (Si–(CH<sub>3</sub>)<sub>2</sub>) groups.  $2905 \text{ cm}^{-1}$  and  $2961 \text{ cm}^{-1}$  (stretching vibration, symmetrical and asymmetrical) of the –CH<sub>3</sub> group. The  $1015 \text{ cm}^{-1}$  peak represents linear Si–O–Si, i.e., growing linear siloxane chains. b) Silica-shell stabilization shows near-identical signatures, minus a small but broad Si–OH ( $3234 \text{ cm}^{-1}$ ) peak, likely from unreacted hydroxyls. Much weaker signatures were noted for the liquid-functionalized variant (red line), albeit present. c) Thermogravimetric analysis of liquid vs vapor-functionalization shows a significantly higher organic loading for the vapor-functionalized variant, over a 2-step degradation. d) Particle diameter coarsens with each vapor-functionalization/stabilization step. e) Growth of DCDMS by vapor deposition creates chains, lengthening and densifying before terminating to give surface chains and/or loops or loose chains and self-terminated loops.

exposure (Figure 2a, red line), evidenced by the early formation of  $809 \text{ cm}^{-1}$ ,  $1264 \text{ cm}^{-1}$ , and  $2961 \text{ cm}^{-1}$  peaks. These represent the rocking and symmetric deformation of the dimethyl (Si–(CH<sub>3</sub>)<sub>2</sub>) and stretching vibration of the methyl (–CH<sub>3</sub>) groups respectively.<sup>[50]</sup> The growing  $2905 \text{ cm}^{-1}$  and  $2961 \text{ cm}^{-1}$  peaks represent increasing growth of –CH<sub>3</sub> groups. The growing  $1015 \text{ cm}^{-1}$  peak represents growing linear Si–O–Si (siloxane) chains.

During excessive reaction (Figure 2a, 960 min, green line), the singular peak at  $1080 \text{ cm}^{-1}$  (Si–O, silica) is co-dominated by a  $1015 \text{ cm}^{-1}$  peak (Si–O–Si, linear siloxanes). This is expected as excessive DCDMS hydrolysis–condensation reaction leads to the formation of silicone oil.<sup>[52]</sup> This is further evidenced by the formation of somewhat oily surfaces (sometimes observable by naked eye). The presence of this silicone oil can be

solvent-extracted and analyzed, showing a gradual increase in eluted oligomeric length as the reaction proceeds (Figure S4, Supporting Information). The minimum wash-out oligomeric chain length detected at 120 minutes (Figure 2a, orange line, and Figure S2 (Supporting Information), optimal liquid repellency) is in the order of  $\approx 700$  repeat units (Figure S4, Supporting Information), which may indicate the length of anchored oligomers ( $<700$  repeat units or  $<112$  nm from a unit length of  $1.6 \text{ \AA}$ ).

The silica-stabilized variant at 120 min (optimum design) is also evaluated against the liquid-functionalized variant (Figure 2b, orange vs red line). Spectroscopic (Figure 2b) and thermogravimetric (Figure 2c) analysis reveal a much lower extent of functionalization with a liquid-phase reaction. Shallower  $809 \text{ cm}^{-1}$  and  $2961 \text{ cm}^{-1}$  peaks (Si-dimethyl (Si-(CH<sub>3</sub>)<sub>2</sub>) and -CH<sub>3</sub>) were observed.  $1015 \text{ cm}^{-1}$  and  $2905 \text{ cm}^{-1}$  peaks (indicative of linear Si-O-Si and densifying -CH<sub>3</sub>) were not observable (Figure 2b). This is notable despite the liquid-functionalized variant achieving superhydrophobicity against pure water.

The enhanced degree of functionalization in vapor-phase is further evidenced by thermogravimetric analysis, with organic content of up to 27.5% w/w vs just 3% w/w with liquid-functionalization (Figure 2c). This significant difference in organic loading is likely the primary reason behind the contrast in performance. For the vapor-functionalized variant, two phases of degradation exist: 1) a volatile component (phase I) which accounts for up to 5% w/w drop until  $300 \text{ }^\circ\text{C}$  and 2) a nonvolatile component that is stable (phase II) until between  $400\text{--}500 \text{ }^\circ\text{C}$  (Figure 2c). This volatile component is likely comprised of loose oligomeric chains,<sup>[53]</sup> which is notably common for chemical vapor functionalized nanoparticles (Figures S5 and S6, Supporting Information).

To understand the influence of volatile vs nonvolatile components on super-liquid-repellency, surfaces (DCDMS, vapor-functionalized) were kept at  $200 \text{ }^\circ\text{C}$  for 24 h before being reassessed (Figure S7 (Supporting Information), spectroscopic a), thermal b), and wetting c,d)). The removal of very minute volatile components ( $<5\%$  w/w) did not lead to degradation in compositional or wetting properties. In fact, performance was marginally improved, as heating is known (but rarely reported<sup>[20,53]</sup>) to improve interfacial chain alignment due to increased molecular mobility. Super-liquid-repellency is thus attributed to the nonvolatile components composed of dimethyl silicone.

The growth of silicone-functionalization can be directly observed by particle size analysis (Figure 2d). Silica shell stabilization increases the median diametric size of native nanoparticles from  $\approx 15$  to  $45 \text{ nm}$  while DCDMS vapor-functionalization results in a final median diametric size of  $\approx 75 \text{ nm}$ . The growth/assembly of silicone functionalization likely occurs via the continuous extension of siloxane chains (Figure 2e). The growth in particle sizes provides a direct observation behind the thermogravimetric- and spectroscopic-analysis of increased organic loading. Within this range of feature sizes, there is likely no direct impact on wettability through the virtue of size ( $10\text{--}100 \text{ nm}$ ),<sup>[54,55]</sup> or geometry (as the particles remain largely as spheroids). Due to the stochastic nature of the reaction, three final silicone configurations likely exist: 1) the loose silicone chains, 2) surface-grafted silicone chains and/or loops, and 3) self-terminated silicone chains. The loose (1) and self-terminated (3) silicone chains make up the non-essential volatile compo-

nents, which can be removed without influencing super-liquid-repellency (Figure S7c,d, Supporting Information). In fact, excessive formation of these loose oligomeric components (oil-like) is observed to degrade super-liquid-repellency (Figure S2, Supporting Information). The growth of nonvolatile surface-grafted dimethyl silicone is therefore likely responsible for the excellent super-liquid-repellency observed.

### 2.3. Performance Limits: Silicone (Methyl/Dimethyl) vs Hydrocarbon vs Perfluoroalkyl Variants

To benchmark performance limits of silicones and hydrocarbons with perfluoroalkyls, vapor- functionalization (Figure 3) of four (three additional) silanes bearing different functionalities were assessed: Trichloromethylsilane (TCMS), trichloro(octyl)silane (OTS), and perfluoro(octyl)silane (PFOTS). After synthesis, these broadly different variants (perfluoroalkyl, hydrocarbon, and silicone) are assessed using FTIR, which confirms the presence or absence of distinctive functional groups: 1) PFOTS, -CF<sub>2</sub> and -CF<sub>3</sub>, 2) OTS, -CH<sub>2</sub> and -CH<sub>3</sub>, and 3) DCDMS, -CH<sub>3</sub> (Figure S8, Supporting Information). Thermogravimetric analysis is also used to gauge the extent of grafting and organic loading in each variant (both vapor- and liquid- functionalized). During vapor-functionalization, DCDMS, TCMS, OTS, and PFOTS were grafted at  $\approx 27.5\%$  w/w,  $14\%$  w/w,  $8\%$  w/w, and  $45\%$  w/w (Figures S5 and S6, Supporting Information) respectively. For long-chain chlorosilanes, i.e., OTS and PFOTS, smaller variations in grafting density between liquid- and vapor-functionalization were noted as compared to the short-chain variants, i.e., DCDMS and TCMS. For long-chain chlorosilanes, there appears to be no direct correlation between organic content vs super-liquid-repellency above a certain organic loading (see Supplementary Discussion, "Performance Limits" and Figure S9, Supporting Information).

Firstly, to assess the importance of crosslinking vs methyl density (Figure 3a vs Figure 3b), trichloromethylsilane (TCMS) was used as a benchmark. The key difference lies in the chain-forming di-methyl group (DCDMS, Figure 3a) vs the cross-linkable trifunctionality mono-methyl group (TCMS, Figure 3b). TCMS trifunctionalization (monomethyl, Figure 3b) enabled super-liquid-repellency down to a surface tension of  $40\text{--}41 \text{ mN m}^{-1}$ . In contrast to this limit, DCDMS-functionalization (dimethyl, Figure 3a) demonstrates a super-liquid-repellency down to  $\approx 32\text{--}33 \text{ mN m}^{-1}$ . Performance contrast (Figure 3a,b) between the dimethyl (-CH<sub>3</sub>)<sub>2</sub> and monomethyl (-CH<sub>3</sub>) variants (DCDMS vs TCMS) reveals the importance of packing functional methyl groups<sup>[53]</sup> at the molecular level (thus also increasing organic loading), particularly under similar degrees of grafting (see Supplementary Discussion, "Performance Limits: TCMS and DCDMS", Supporting Information). The performance of dimethyl silicone vs perfluoroalkyl (see below) is attributed to the near-matching of effective surface energy (dimethyl silicone:  $19\text{--}21 \text{ mJ m}^{-2}$ <sup>[41]</sup> vs perfluoroalkyl:  $11\text{--}19 \text{ mJ m}^{-2}$ <sup>[41]</sup>). This results in similar levels of super-liquid-repellency against the partially polar test liquids.

Secondly, to benchmark performance against state-of-the-art long-chain trichlorosilanes, OTS and PFOTS are cross-compared. The functionalization of hydrocarbon (-CH<sub>2</sub> and -CH<sub>3</sub>) chains (OTS, Figure 3c,d) allowed super-liquid-repellency

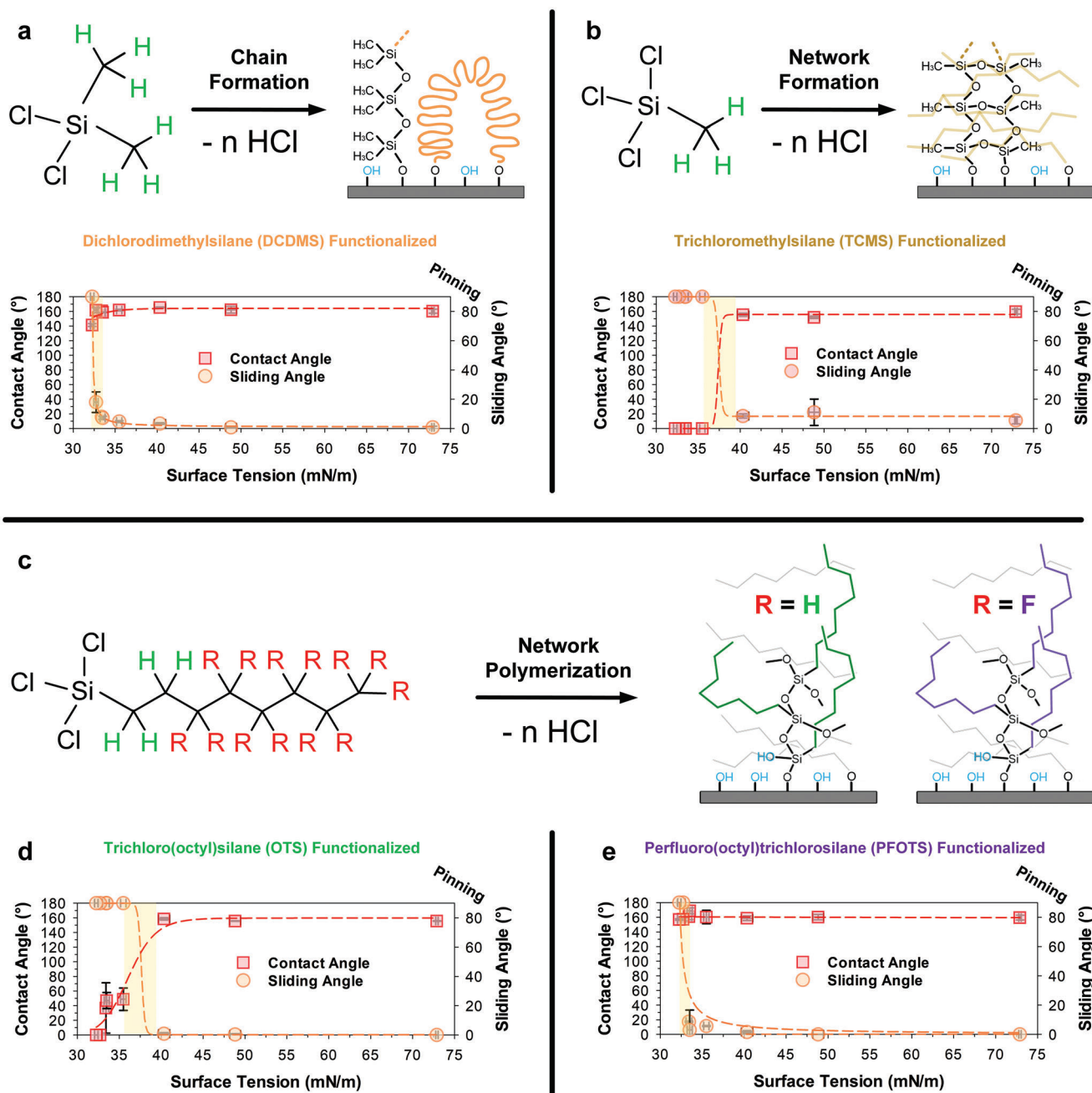


**Figure 3.** Benchmarking: Silicones (monomethyl and dimethyl) vs hydrocarbon vs perfluoroalkyl ( $n = 3$ , mean  $\pm$  standard deviation). a) DCDMS-functionalization achieves a super-liquid-repellency down to  $\approx 32\text{--}33 \text{ mN m}^{-1}$ . b) TCMS functionalization achieves a diminished performance ( $\approx 40\text{--}41 \text{ mN m}^{-1}$ ). c) Commonly used hydrophobic  $\text{C}_8$  trichlorosilanes (trichloro(octyl)silane, OTS, and perfluoro(octyl)silane, PFOTS) were also benchmarked. d) OTS achieves a super-liquid-repellency down to  $\approx 40\text{--}41 \text{ mN m}^{-1}$ . e) PFOTS achieves the best (expectedly) level of super-liquid-repellency, at down to  $\approx 31\text{--}32 \text{ mN m}^{-1}$ . Schematized chain lengths are not to scale.

to reach  $\approx 40\text{--}41 \text{ mN m}^{-1}$ , matching the performance by TCMS. This level of performance is surprising, considering that OTS-functionalized superhydrophobicity is rarely assessed beyond the use of pure water.<sup>[35,36]</sup> The functionalization of perfluoroalkyl ( $-\text{CF}_2$  and  $-\text{CF}_3$ ) chains (PFOTS, Figure 3c,e) results in super-liquid-repellency of down to  $\approx 31\text{--}32 \text{ mN m}^{-1}$ . In subsequent testing (Figure 4), the perfluoroalkyl functionalization was even capa-

ble of repelling hexadecane ( $27.4 \text{ mN m}^{-1}$ ) but fails (liquid drops pin) with cyclohexane ( $25.0 \text{ mN m}^{-1}$ ) or decane ( $23.8 \text{ mN m}^{-1}$ ). This is intriguing as it almost matches performance attained using specific surface structuring (without dense functionalization at  $\approx 1\text{--}5\%$  w/w functionalized)<sup>[22]</sup> or much denser in-liquid surface functionalization (without specific surface structuring at  $\approx 45\%$  w/w functionalized).<sup>[19]</sup>

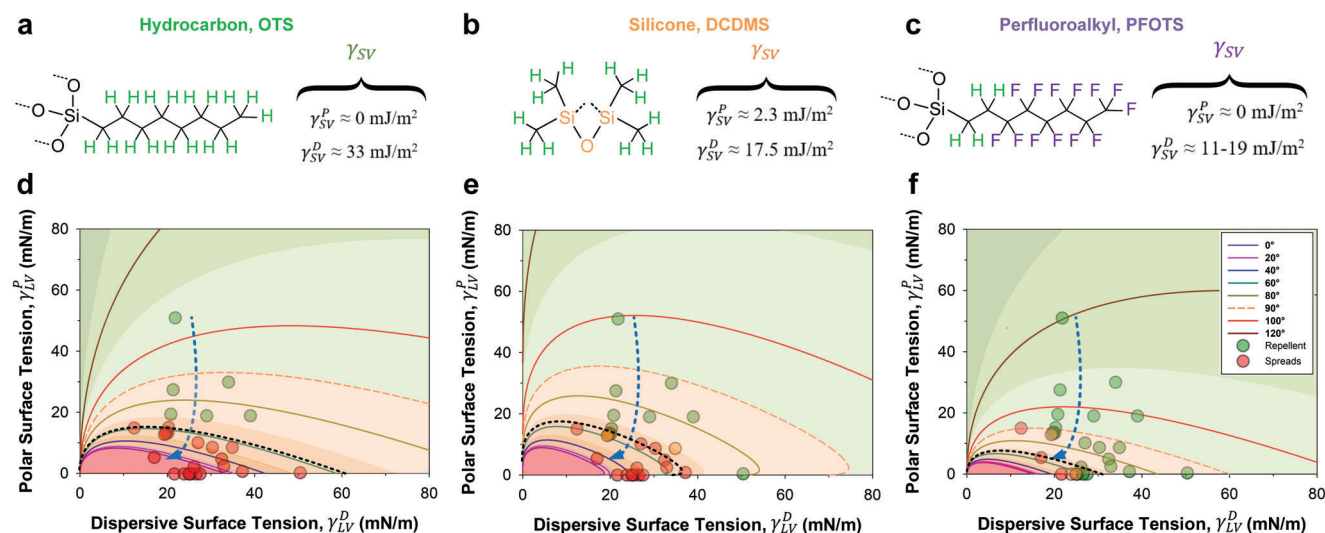


**Figure 4.** Predictive design: Surface chemistry vs super-liquid repellency. a–c) Surface chemistries: a) hydrocarbon-functionalized (via OTS), b) dimethylsilicone-functionalized (via DCDMS), and c) perfluoroalkyl-functionalized (via PFOTS). Surface energy components (polar and non-polar, i.e., dispersive) are collated from the literature.<sup>[40,56–58]</sup> d–f) Solving the OWRK equation generates wetting envelope plots, with zones (green, orange, and red) depicting error domains ( $\pm 10^\circ$ , bracketing each solid line) arising from different liquid properties: x-axis (dispersive  $\gamma_{LV}^D$ ) and y-axis (polar  $\gamma_{LV}^p$ ). In combination with the Wenzel limit ( $90^\circ$ , dashed orange line), the domain of failure is highlighted (dark orange to red). The black dashed line represents a best-fit envelope (minimum rms error) that is defined around the domain of failure (between orange and red data points). Tetrahydrofuran was excluded from this analysis for (f) due to its anomalous nature. The dashed blue arrow indicates the model test liquid: ethanol–water mixtures. Liquid mixture properties are defined in accordance to the literature.<sup>[59,60]</sup> Experimental results from liquid drop repellency tests show that super-liquid-repellency is lost far below the Wenzel limit. Marker legends: 1) green: sliding drops, 2) orange: pinning drops, and 3) red: superspreading drops.

#### 2.4. Predicting Superwettability: Surface Chemistry vs Super-Liquid-Repellency

The super-liquid-repellency limits () for the fluoro-free variants already transcend many current state-of-the-art descriptions for fluoro-free functionalities (Figure 3 and Table S2, Supporting Information). To improve mechanistic understanding while enabling the prediction of super-liquid-repellency limits, we now consider models describing polar to non-polar liquid–solid interactions alongside empirical observations.

The Owens–Wendt–Rabel–Kaelble (OWRK) model<sup>[61,62,63]</sup> is often used to describe the relationship between liquid surface tension ( $\gamma_{LV}$ ), solid surface energy ( $\gamma_{SV}$ ), through the inherent (Young’s) liquid-on-solid contact angle ( $\theta_{\text{inherent}}$  or  $\theta_{\text{adv}}$ ). The two-parameter model considers additional liquid–solid interactions between the non-polar (dispersive) and polar components using a harmonic mean (see Supplementary Discussion, “OWRK Model”, Supporting Information).<sup>[61–64]</sup> For a liquid, the effective surface tension, is represented as a combination of  $\gamma_{LV}^D$ , e.g. non-polar or London dispersion forces and polar interactions,  $\gamma_{LV}^p$ , e.g. dipole interactions,  $\gamma_{LV} = \gamma_{LV}^D + \gamma_{LV}^p$ . Analogously, the effective solid surface energy is  $\gamma_{SV} = \gamma_{SV}^D + \gamma_{SV}^p$ . Based on these parameters, the OWRK model attempts to describe the wetting behavior of a liquid on a solid as follows:

$$\gamma_{LV} (1 + \cos(\theta_{\text{inherent}})) = 2 \left[ \sqrt{(\gamma_{SV}^D \gamma_{LV}^D)} + \sqrt{(\gamma_{SV}^p \gamma_{LV}^p)} \right] \quad (1)$$

Important assumptions include being of a pure liquid on a perfectly smooth solid (topographically and chemically homoge-

nous) without chemical reaction. Experimentally measured contact angles,  $\theta$ , will not easily satisfy these assumptions.<sup>[65]</sup> To provide a qualitative understanding of model accuracy, solutions to Equation (1) are verified by using multiple modes of contact angle measurements ( $\theta$ , static contact angle, alongside both  $\theta_{\text{adv}}$  and  $\theta_{\text{rec}}$ , advancing and receding contact angle) from both literature and in-house measurements (Figure S10, Supporting Information). Errors are often range-bounded by  $\approx \pm 10^\circ$ , although larger errors (up to  $20^\circ$ ) do exist. This is expected as the OWRK equation is affected by accurate contact angle measurements.<sup>[66]</sup> However, it remains capable of predicting broad wetting trends (Figure S10, Supporting Information) across significantly different surface energies (i.e.,  $\Delta\gamma_{SV} \approx 10 \text{ mJ m}^{-2}$ ).

Solving the OWRK equation (see Supplementary Discussion, “OWRK Model”, Supporting Information) estimates the static wetting properties (contact angle,  $\theta$ ) via known non-polar (dispersive) and polar components of target liquids and solids. Notably, while hydrocarbon-based ( $-\text{CH}_2$  and  $-\text{CH}_3$ ) and perfluoroalkyl-based ( $-\text{CF}_2$  and  $-\text{CF}_3$ ) chemistries are known to be predominantly dispersive (D) in nature ( $\gamma_{SV}^p/\gamma_{SV}^D \approx 0.01$ ),<sup>[41,57,58]</sup> the siloxane-bounded  $-\text{CH}_3$  of dimethyl silicone,  $[\text{O}-\text{Si}(\text{CH}_3)_2]_x$ , possesses a non-trivial polar (P) component ( $\gamma_{SV}^p/\gamma_{SV}^D \approx 0.13$ ).<sup>[56]</sup>

Using known literature values<sup>[41,56–58]</sup> of  $\gamma_{SV}^D$  and  $\gamma_{SV}^p$  (Table S3, Supporting Information) for hydrocarbon, dimethyl silicone, and perfluoroalkyl (Figure 4a–c), OWRK wetting envelope plots (i.e., wetting profiles) are generated. These are further converted into phase diagrams with each contour line (estimated  $\theta$ ) being bracketed by a typical  $\pm 10^\circ$  error range (Figure 4d–f, shaded domains). Liquid properties are denoted along the x-axis (dispersive  $\gamma_{LV}^D$ ) and y-axis (polar  $\gamma_{LV}^p$ ). To test each surface’s

limit in super-liquid-repellency, 20 probe liquids with known  $\gamma_{LV}^D$  and  $\gamma_{LV}^P$  were assessed (Table S4, Supporting Information). The ability to roll-off a 10  $\mu$ L liquid drop at 10° tilt angle is considered super-liquid-repellent and assigned a green marker on the OWRK phase diagrams. Pinned (but not superspreading) and superspreading drops are assigned orange and red markers, respectively (Table S5, Supporting Information).

For hydrocarbon-functionalized (OTS) surfaces, failure of super-liquid-repellency was found far below the Wenzel-limit (Figure 4d, moderate to dark orange zones). For dimethyl silicone functionalized (DCDMS) surfaces, we observe an even smaller failure window (Figure 4e). For perfluoroalkyl-functionalized (PFOTS) surfaces, the smallest failure window exists (Figure 4f). All 3 variants had a domain of failure within the moderate to dark orange zones (modeled of 60°–70°, Figure 4d–f, green lines). Deviation from the model green lines is depicted by the black dashed envelope. These modeled failure windows are well-aligned with the experimentally measured range of contact angles ( $\theta$  of 60°  $\pm$  10°, Figure S10d–i, green lines, Supporting Information). Notably, only 1 specific liquid-surface combination (out of 60 tests) fell significantly out-of-phase: tetrahydrofuran ( $\gamma_{LV}^D = 12.4$ ,  $\gamma_{LV}^P = 15$ ) on PFOTS-functionalized nanoparticles. The reasons are yet unknown. Considering the high success rate of estimating super-liquid-repellency above this failure window (modeled of 60°–70°), predicting performance with new liquids (or mixtures) may be possible. Above a Wenzel-limit of 90°, super-liquid-repellency is guaranteed (Figure 4d–f, green zones). Below the Wenzel-limit of 90°, super-liquid-repellency is still largely possible (Figure 4d–f, light to moderate orange zones, >70°). Failure of super-liquid-repellency is likely to occur within the red zones (Figure 4d–f, <60°), with a transition between 60°–70° (dark orange zones).

DCDMS or dimethyl silicone performs better than hydrocarbon (OTS) or monomethyl silicone (TCMS) under all situations. The critical failure behavior with purely dispersive (non-polar liquids) with hydrocarbon- and silicone-functionalities occurs earlier than with polar liquids. This occurs despite having similar net effective surface tensions. Qualitatively, this is attributed to the nature of chemical affinity/compatibility<sup>[67]</sup> between surface and liquid chemistry. Hydrocarbon- and silicone-functionalities are molecularly similar to hydrocarbon-based liquids, unlike perfluoroalkyls. Therefore, with the former variants, predominantly polar aqueous liquids can be repelled while predominantly non-polar hydrocarbon-based liquids cannot be repelled. Quantitatively, this effect is adequately captured by the OWRK model (see Supplementary Discussion, "Non-Polar Liquids", Supporting Information).

To test this concept, the model test liquids: ethanol–water mixtures were assessed. The polar and non-polar (or dispersive) properties are estimated using a binary model<sup>[59,60]</sup> (Table S4\*, Supporting Information). They are then compiled into Figure 4d–f, as per the blue dashed arrows, showing excellent estimates of super-liquid-repellency limits. OTS, DCDMS, and PFOTS transitioned to failure at modeled of  $\approx$ 60°, 65°, and 65° respectively. The conceptual use of these phase diagrams (for both sprayed nanoparticles and/or otherwise) can be useful in guiding the future of sustainably designed (fluoro-free) super-liquid-repellency per basis of requirements (liquid properties).

## 2.5. Deviation from Cassie / Wenzel's Hydrophobicity Limit of 90°

In the pioneering studies of Cassie–Baxter and Wenzel,<sup>[66,67]</sup> the demarcation of (super)hydrophilicity-to-(super)hydrophobicity lies at  $\approx$  90°. This limit is clearly violated here ( $\theta_{\text{transition}}$  of 60°–70°). In this study, two hypothetical causes may exist: 1) Hydrophobic attraction, which is attributed to a range of real-world phenomena that the Cassie–Baxter and Wenzel models do not consider (see Supplementary Discussion, "Deviation from Cassie Limits", Supporting Information). 2) Spontaneous re-entrancy, which could be formed by the presence of nanoparticle agglomerates. Perfect spheres, for instance, are known to exhibit a significant degree of re-entrancy ( $\alpha$ ), down to  $\alpha = 60^\circ$  supporting a  $\alpha = 30^\circ$ .<sup>[68]</sup> While fumed silica nanoparticles do not possess perfect spherical geometries, localities with re-entrant overhangs may still be distributed stochastically. These spontaneously occurring overhangs are instrumental in preserving the Cassie-state. While both factors may contribute to the as-observed Wenzel-limit deviation, spontaneous re-entrancy likely dominates. This is attributed to the macroscopic effect imposed on the contact line by re-entrancy, contrasting the (comparatively smaller) nanoscopic influence exerted by hydrophobic attraction.

## 2.6. Real-World Use of Hydrocarbon, Dimethyl Silicone, and Perfluoroalkyl Surface Chemistries

The real-world assessment of fluoro-free super-liquid-repellent surfaces is illustrated by functional in-air liquid repellency and under-immersion functionality with model contaminated liquids. Some of the world's most contaminated liquids are aqueous-based, including wastewater with soaps, surfactants, and oils having an effective range of surface tensions from 30–60 mN m<sup>-1</sup>.<sup>[72]</sup> Therefore, a series of model contaminated liquids were designed: 1) Oily-water: hexadecane (2 mL): water (2 mL): CTAB-1 CMC (1 mL) at 56 mN m<sup>-1</sup> (the typical range of wastewater), 2) Cationic (Cetyltrimethylammonium bromide, CTAB) and anionic surfactants (Sodium dodecyl sulfate, SDS) at 1 CMC,  $\approx$  36.6 mN m<sup>-1</sup> and 37.2 mN m<sup>-1</sup>, respectively, 3) An ethanol–water mixture ( $\gamma \approx$  32–33 mN m<sup>-1</sup>) is also included for reference. All vapor-functionalized variants (hydrocarbon, dimethyl silicone, and perfluoroalkyl) exhibit excellent super-liquid-repellency against water, oil–water, and the anionic soap (SDS at 1 CMC). However, only the dimethyl silicone (DCDMS) and perfluoroalkyl (PFOTS) variants were able to repel liquids with lower surface tensions: 1) cationic soap (CTAB at 1 CMC) and 2) ethanol–water mixture ( $\approx$  32–33 mN m<sup>-1</sup>) (Figure 5a,b).

To probe the drop impact repellency of hydrocarbon (OTS), dimethyl silicone (DCDMS), and perfluoroalkyl (PFOTS) functionalization, the in-air drop impact of pure water and ethanol–water drops ( $\approx$  40–41 mN m<sup>-1</sup>) was performed. Repellency was assessed using contact time analysis. Contact time was assessed from the point of drop-to-surface contact to the point of drop-from-surface departure (Figure 5c). With pure water, DCDMS and PFOTS are comparatively more consistent vs OTS (Figure 5d, smaller stochastic spread of contact times). With ethanol–water ( $\gamma \approx$  40–41 mN m<sup>-1</sup>), the contact time appears to occur over a larger stochastic spread for all 3 variants. However,

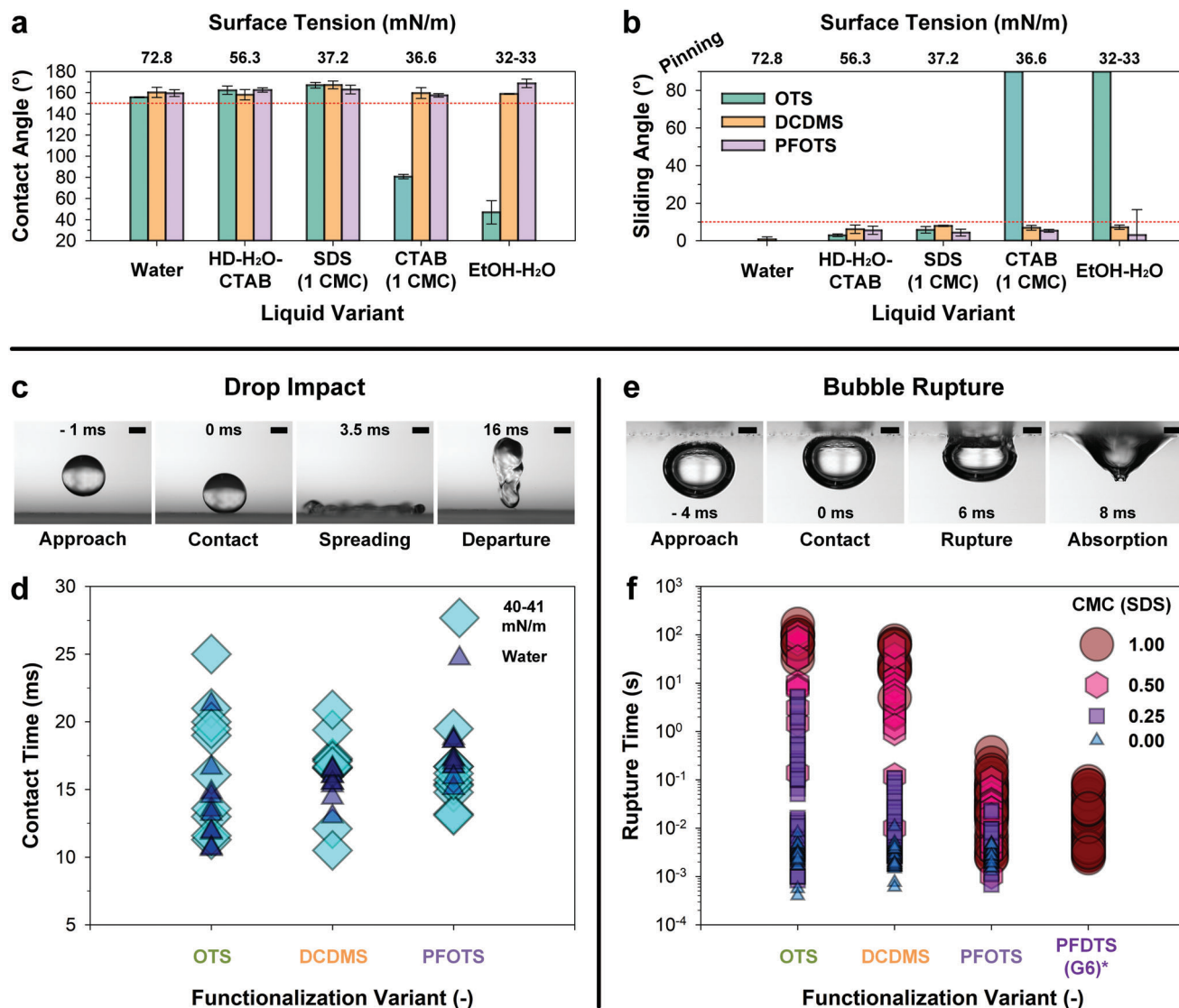


**Figure 5.** Use and limitations: Super-liquid-repelling of hydrocarbon (OTS, green), dimethyl silicone (DCDMS, orange), and perfluoroalkyl functionalization (PFOTS, purple). a,b) Clean water, model oil–water emulsion (hexadecane–water–CTAB mixture), SDS at 1 CMC, CTAB at 1 CMC, and ethanol-in-water (32–33 mN m<sup>-1</sup>) were assessed ( $n = 3$ , mean  $\pm$  standard deviation) for contact angles (a) and sliding angles (b). Surface tensions are included in the top axis. c) Drop impact testing ( $n = 10$ ) with clean water and ethanol-in-water (40–41 mN m<sup>-1</sup>), shows d) a weak correlation between surface chemistry and contact time. e) Bubble rupture testing ( $n = 20$ –50) under immersion with variable SDS concentration (0–1 CMC), shows f) a strong correlation between surface chemistry and rupture time, ranging over 7 orders in magnitude. For reference, a known optimized variant of heavily perfluorinated silica nanoparticles (PFDTs, G6)<sup>69,70</sup> is also assessed at 1 CMC for reference. Scale bar: 1 mm.

the spread is the largest for OTS, followed by DCDMS, and the smallest for PFOTS. This is attributed to decreased interaction forces from the latter, leading to lower adhesion/dissipation, and thus contact time. Albeit a weak correlation, this is indicative of effective liquid impact repellency in the following order: PFOTS > DCDMS  $\geq$  OTS.

As a harsher test of super-liquid-repelling, the plastron stability of hydrocarbon (OTS), dimethyl silicone (DCDMS), and perfluoroalkyl (PFOTS) functionalization was assessed. This was performed via under-water bubble rupture of SDS solutions (0 to 1 CMC) (Figure 5e). The rupture time is determined by the time between bubble contact and the peak velocity induced by absorption, as defined in earlier works.<sup>69,70</sup> The ability to absorb bub-

bles under-water during immersion is a harsher and more sensitive probe compared to in-air drop impact. This is evidenced by the extent of stochastic spread in bubble rupture timings to over 7 orders of magnitudes (from milliseconds to hundreds of seconds, Figure 5f). With the use of pure water, 0 CMC (Figure 5f, blue triangles), the bubble rupture time distributions for all variants are similar. With an increased concentration of surfactants, at 0.25 CMC (Figure 5f, purple squares), the spread of rupture times increases for all variants, with OTS > DCDMS > PFOTS. This trend continues to increase with 0.50 CMC (Figure 5f, pink hexagons) and 1.00 CMC (Figure 5f, brown circles).

During immersion, long equilibrium interaction time (minutes) facilitates the stabilization of thin liquid films on

surfaces.<sup>[72,73]</sup> The ability to rupture this film (hence the bubble) requires sufficiently strong interaction forces<sup>[74]</sup> to act between the solid–gas (nanoparticle–air) and the opposing gas phase (bubble) through the liquid (surfactant-laced water). These forces induce film thinning-and-rupture.<sup>[75,76]</sup>

Changing the liquid composition (by surfactant concentration) or solid surface chemistry alters these interaction forces (solid/gas–liquid–gas composite). Surfactants will also impose non-slip boundary conditions that further slows down the hydrodynamic drainage of the film.<sup>[75,76]</sup> Hydrocarbon chemistry (from OTS, with numerous methylene groups,  $-\text{CH}_2$ ) is chemically/energetically very similar to the surfactants (long  $-\text{CH}_2$  hydrocarbon tails) present in the SDS solution. As a result, it promotes stabilizing interactions that maintain the thin film between the bubble and the solid phase. Silicone chemistry (from DCDMS, with only dimethyl groups,  $(-\text{CH}_3)_2$ ) is chemically/energetically more dissimilar to the surfactants, thus conferring less stability. Perfluoroalkyl chemistry (from PFOTS, with difluoromethylene ( $-\text{CF}_2$ ) and trifluoromethyl ( $-\text{CF}_3$ ) groups) is chemically/energetically very different from the hydrocarbon-based surfactant chains. Therefore, interactions between the perfluoro-alkylated solid and the gas phase in the bubble promote the greatest thin film destabilization potential and thus result in comparatively rapid bubble rupture.

At 1.00 CMC, this surface-chemistry-directed trend is further verified using a second control surface known for a very high perfluoroalkyl content<sup>[19]</sup> and exemplary bubble rupturing properties (Figure 5f, PFDTS (G6)\*).<sup>[69,70]</sup> In alignment with theories that govern thin film stability of impure water,<sup>[75–77]</sup> the dimethyl silicone functionality performs in accordance with its uniquely intermediate surface energy properties, falling between hydrocarbon and perfluoroalkyl. Among the fluoro-free super-liquid-repellent variants, dimethyl silicone functionalization offers the greatest performance-to-sustainability ratio. We maintain the use of perfluoroalkyl chemistry under highly specialized situations but would encourage the exploration of fluoro-free chemistry (albeit limitations) for many other common applications.

### 3. Conclusion

Most real-world contaminated liquids are aqueous-based, having low to moderate effective surface tensions (30–60 mN m<sup>-1</sup>). Notably, the effective surface tension is (often) composed of co-dominating non-polar (dispersive) and polar components. Understanding this enables the design of surfaces capable of low-surface-tension super-liquid-repellency without the use of perfluoroalkyls (a persistent environmental and bioaccumulation hazard). To predict the limits of super-liquid-repellency for different surface chemistries, wetting envelopes with functional phase domains are developed and empirically verified. For a system of stochastically formed nanoparticles, a critical transition exists at  $60^\circ < < 70^\circ$  for almost any target liquid. The future design of super-liquid-repellency should be liquid-centric, i.e., tailored to target liquid properties. We hope that these findings would encourage prudent and non-pollutive surface chemistry designs. The highly performing fluoro-free dimethyl  $(-\text{CH}_3)_2$  silicone functionality (vs monomethyl silicones and aliphatic hydro-

carbons) is likely attributed to its denser dimethylated configuration ( $[\text{O}-\text{Si}(\text{CH}_3)_2]_x$ ). Notwithstanding purely non-polar (dispersive) hydrocarbon oils or solvents, many aqueous-based liquids can be repelled by fluoro-free surface chemistries. Understanding these design principles is key to the future of sustainably achieved super-liquid-repellency.

## 4. Experimental Section

Details of all experiments are included in the Supporting Information (Synthesis and Characterization).

## Supporting Information

Supporting Information is available from the Wiley Online Library or from the author.

## Acknowledgements

This work had been supported by the European Union's HORIZON research and innovation program under the Marie Skłodowska-Curie grant agreement No. 101062409 and the Academy of Finland grant agreement No. 13347247 (W.S.Y.W). The authors acknowledge support by the Tandem Industry Academia funding from the Finnish Research Impact Foundation project No. 239 (R.H.A.R. and M.S.K.). This work was also supported by the Academy of Finland (Center of Excellence Program (2022–2029)) in Life-Inspired Hybrid Materials (LIBER) project number 346109 and Academy of Finland Project number 342169 (R.H.A.R.). The authors also acknowledge the provision of facilities and technical support by Aalto University at the OtaNano Nanomicroscopy Center. The authors thank K. Liu, X. Tian, S. Lepikko, M. Rodriguez-Valverde, D. Vollmer, A. Naga, H. Kusumaatmaja, L. Hauer, A. Marmur, and V. Craig for the inspiring discussions.

## Conflict of Interest

The authors declare no conflict of interest.

## Author Contributions

W.S.Y.W. designed the experiments, analyzed the data, and prepared the manuscript. M.S.K. perform some of the wetting experiments to confirm cross-testing reproducibility and performed optical profiling on different surfaces. S. Z. performed and analyzed results from transmission electron microscopy. M.J. helped in performing measurements and understanding the FTIR data. L.K. helped perform the size exclusion gel permeation chromatography alongside data analysis. W.S.Y.W. and R.H.A.R. planned and wrote the manuscript. All authors reviewed and approved the manuscript.

## Data Availability Statement

The data that support the findings of this study are available from the corresponding authors upon reasonable request.

## Keywords

polar and dispersive interactions, predicting superwettability, super-liquid-repellent surfaces, superhydrophobic materials, surface chemistry

Received: January 10, 2023  
Revised: April 4, 2023  
Published online: June 1, 2023

- [1] A. K. Kota, G. Kwon, A. Tuteja, *NPG Asia Mater.* **2014**, *6*, e109.
- [2] T. L. Liu, C.-J. C. Kim, *Science* **2014**, *346*, 1096.
- [3] A. Lafuma, D. Quere, *Nat. Mater.* **2003**, *2*, 457.
- [4] L. Jiang, Y. Zhao, J. Zhai, *Angew. Chem., Int. Ed.* **2004**, *43*, 4338.
- [5] A. Tuteja, W. Choi, G. H. McKinley, R. E. Cohen, M. F. Rubner, *MRS Bull.* **2008**, *33*, 752.
- [6] X. Deng, L. Mammen, H.-J. Butt, D. Vollmer, *Science* **2012**, *335*, 67.
- [7] J. Zhang, S. Seeger, *Angew. Chem., Int. Ed.* **2011**, *50*, 6652.
- [8] K. K. S. Lau, J. Bico, K. B. K. Teo, M. Chhowalla, G. A. J. Amaratunga, W. I. Milne, G. H. McKinley, K. K. Gleason, *Nano Lett.* **2003**, *3*, 1701.
- [9] A. Grigoryev, I. Tokarev, K. G. Kornev, I. Luzinov, S. Minko, *J. Am. Chem. Soc.* **2012**, *134*, 12916.
- [10] S. M. Kang, S. M. Kim, H. N. Kim, M. K. Kwak, D. H. Tahk, K. Y. Suh, *Soft Matter* **2012**, *8*, 8563.
- [11] K. Golovin, D. H. Lee, J. M. Mabry, A. Tuteja, *Angew. Chem., Int. Ed.* **2013**, *52*, 13007.
- [12] S. Pan, A. K. Kota, J. M. Mabry, A. Tuteja, *J. Am. Chem. Soc.* **2013**, *135*, 578.
- [13] G.-T. Yun, W.-B. Jung, M. S. Oh, G. M. Jang, J. Baek, N. I. Kim, S. G. Im, H.-T. Jung, *Sci. Adv.* **2018**, *4*, eaat4978.
- [14] R. Hensel, R. Helbig, S. Aland, H.-G. Braun, A. Voigt, C. Neinhuis, C. Werner, *Langmuir* **2013**, *29*, 1100.
- [15] A. Tuteja, W. Choi, J. M. Mabry, G. H. McKinley, R. E. Cohen, *Proc. Natl. Acad. Sci. USA* **2008**, *105*, 18200.
- [16] T. Nishino, M. Meguro, K. Nakamae, M. Matsushita, Y. Ueda, *Langmuir* **1999**, *15*, 4321.
- [17] D. Wang, Q. Sun, M. J. Hokkanen, C. Zhang, F.-Y. Lin, Q. Liu, S.-P. Zhu, T. Zhou, Q. Chang, B. He, Q. Zhou, L. Chen, Z. Wang, R. H. A. Ras, X. Deng, *Nature* **2020**, *582*, 55.
- [18] F. Geyer, M. D'Acunzi, A. Sharifi-Aghili, A. Saal, N. Gao, A. Kaltbeitzel, T.-F. Sloot, R. Berger, H.-J. Butt, D. Vollmer, *Sci. Adv.* **2020**, *6*, eaaw9727.
- [19] W. S. Y. Wong, *Nano Lett.* **2019**, *19*, 1892.
- [20] W. S. Y. Wong, Z. H. Stachurski, D. R. Nisbet, A. Tricoli, *ACS Appl. Mater. Interfaces* **2016**, *8*, 13615.
- [21] W. S. Y. Wong, G. Liu, N. Nasiri, C. Hao, Z. Wang, A. Tricoli, *ACS Nano* **2016**, *11*, 587.
- [22] C. Peng, Z. Chen, M. K. Tiwari, *Nat. Mater.* **2018**, *17*, 355.
- [23] S. Pan, R. Guo, M. Björnmalin, J. J. Richardson, L. Li, C. Peng, N. Bertleff-Zieschang, W. Xu, J. Jiang, F. Caruso, *Nat. Mater.* **2018**, *17*, 1040.
- [24] Y. Lu, S. Sathasivam, J. Song, C. R. Crick, C. J. Carmalt, I. P. Parkin, *Science* **2015**, *347*, 1132.
- [25] X. Lim, *Nature* **2019**, *566*, 26.
- [26] R. Lohmann, I. T. Cousins, J. C. DeWitt, J. Glüge, G. Goldenman, D. Herzke, A. B. Lindstrom, M. F. Miller, C. A. Ng, S. Patton, M. Scherlinger, X. Trier, Z. Wang, *Environ. Sci. Technol.* **2020**, *54*, 12820.
- [27] R. C. Buck, J. Franklin, U. Berger, J. M. Conder, I. T. Cousins, P. de Voogt, A. A. Jensen, K. Kannan, S. A. Mabury, S. P. van Leeuwen, *Integr. Environ. Assess. Manage.* **2011**, *7*, 513.
- [28] J. Han, L. Kiss, H. Mei, A. M. Remete, M. Ponikvar-Svet, D. M. Sedgwick, R. Roman, S. Fustero, H. Moriwaki, V. A. Soloshonok, *Chem. Rev.* **2021**, *121*, 4678.
- [29] M. G. Evich, M. J. B. Davis, J. P. McCord, B. Acrey, J. A. Awkerman, D. R. U. Knappe, A. B. Lindstrom, T. F. Speth, C. Tebes-Stevens, M. J. Strynar, Z. Wang, E. J. Weber, W. M. Henderson, J. W. Washington, *Science* **2022**, *375*, eabg9065.
- [30] B. Trang, Y. Li, X.-S. Xue, M. Ateia, K. N. Houk, W. R. Dichtel, *Science* **2022**, *377*, 839.
- [31] V. Dichiarante, M. I. Martinez Espinoza, L. Gazzera, M. Vuckovac, M. Latikka, G. Cavallo, G. Raffaini, R. Oropesa-Nuñez, C. Canale, S. Dante, S. Marras, R. Carzino, M. Prato, R. H. A. Ras, P. Metrangolo, *ACS Sustainable Chem. Eng.* **2018**, *6*, 9734.
- [32] *Chemicals Strategy for Sustainability Towards a Toxic-Free Environment*, [https://ec.europa.eu/environment/pdf/chemicals/2020/10/SWD\\_PFAS.pdf](https://ec.europa.eu/environment/pdf/chemicals/2020/10/SWD_PFAS.pdf) (accessed: January 2023).
- [33] S. Shabaniyan, B. Khatir, A. Nisar, K. Golovin, *Nat. Sustainability* **2020**, *3*, 1059.
- [34] Q. Fu, J. Han, X. Wang, P. Xu, T. Yao, J. Zhong, W. Zhong, S. Liu, T. Gao, Z. Zhang, L. Xu, B. Song, *Adv. Mater.* **2021**, *33*, 1907818.
- [35] S. R. Saeid Jalali, S. Sobat, G. Farzi, *Mater. Res. Express* **2018**, *5*, 095311.
- [36] N. J. Janowicz, H. Li, F. L. Heale, I. P. Parkin, I. Papakonstantinou, M. K. Tiwari, C. J. Carmalt, *Langmuir* **2020**, *36*, 13426.
- [37] M. Long, S. Peng, X. Yang, W. Deng, N. Wen, K. Miao, G. Chen, X. Miao, W. Deng, *ACS Appl. Mater. Interfaces* **2017**, *9*, 15857.
- [38] H. Luo, M. Yang, D. Li, Q. Wang, W. Zou, J. Xu, N. Zhao, *ACS Appl. Mater. Interfaces* **2021**, *13*, 13813.
- [39] K. S. Choudhari, S. D. Kulkarni, S. Chidangil, S. D. George, *Bull. Mater. Sci.* **2020**, *43*, 193.
- [40] S. M. Kirk, M. A. Strobel, C.-Y. Lee, S. J. Pachuta, M. J. Prokosch, H. L. Lechuga, M. E. Jones, C. S. Lyons, S. Degner, Y. Yang, M. J. Kushner, *Plasma Processes Polym.* **2010**, *7*, 107.
- [41] J. E. Mark, *Polymer Data Handbook*, Oxford University Press, New York, **1999**.
- [42] C. Capello, U. Fischer, K. Hungerbühler, *Green Chem.* **2007**, *9*, 927.
- [43] K. Duarte, C. I. L. Justino, A. M. Gomes, T. Rocha-Santos, A. C. Duarte, in *Analysis of Marine Samples in Search of Bioactive Compounds, Comprehensive Analytical Chemistry*, vol. 65 (Eds: T. Rocha-Santos, A. C. Duarte), Elsevier, New York **2014**, pp. 59–78.
- [44] P. S. Brown, B. Bhushan, *APL Mater.* **2016**, *4*, 015703.
- [45] R. Campos, A. J. Guenther, T. S. Haddad, J. M. Mabry, *Langmuir* **2011**, *27*, 10206.
- [46] R. Campos, A. J. Guenther, A. J. Meuler, A. Tuteja, R. E. Cohen, G. H. McKinley, T. S. Haddad, J. M. Mabry, *Langmuir* **2012**, *28*, 9834.
- [47] L. Boksányi, O. Liardon, E. S. Kováts, *Adv. Colloid Interface Sci.* **1976**, *6*, 95.
- [48] D. W. Sindorf, G. E. Maciel, *J. Phys. Chem.* **1982**, *86*, 5208.
- [49] J. J. Shephard, A. K. Soper, S. K. Callear, S. Imberti, J. S. O. Evans, C. G. Salzmann, *Chem. Commun.* **2015**, *51*, 4770.
- [50] Z. Daneshfar, F. Goharpey, J. K. Yeganeh, *Mater. Res. Express* **2018**, *5*, 095005.
- [51] J. Liu, Y. Sun, X. Zhou, X. Li, M. Kappl, W. Steffen, H.-J. Butt, *Adv. Mater.* **2021**, *33*, 2100237.
- [52] I. Hasegawa, Y. Nakane, T. Takayama, *Appl. Organomet. Chem.* **1999**, *13*, 273.
- [53] M. J. Owen, *Macromol. Rapid Commun.* **2021**, *42*, 2000360.
- [54] C. Dorner, J. Rühle, *Beilstein J. Nanotechnol.* **2011**, *2*, 327.
- [55] Q. Zheng, C. Lü, *Procedia IUTAM* **2014**, *10*, 462.
- [56] S. Wu, *J. Polym. Sci., Part C: Polym. Symp.* **1971**, *34*, 19.
- [57] E. Lindner, E. Arias, *Langmuir* **1992**, *8*, 1195.
- [58] K. Mader-Arndt, Z. Kutelova, R. Fuchs, J. Meyer, T. Stedler, W. Hintz, J. Tomas, *Granul. Matter* **2014**, *16*, 359.
- [59] Z. Zhang, W. Wang, A. N. Korpacz, C. R. Dufour, Z. J. Weiland, C. R. Lambert, M. T. Timko, *Langmuir* **2019**, *35*, 12317.
- [60] A. Jarray, V. Magnanimo, S. Luding, *Powder Technol.* **2019**, *341*, 126.
- [61] W. Rabel, *Farbe und Lack* **1971**, *77*, 997.
- [62] D. H. Kaelble, *J. Adhes.* **1970**, *2*, 66.
- [63] D. K. Owens, R. C. Wendt, *J. Appl. Polym. Sci.* **1969**, *13*, 1741.
- [64] L. A. Girifalco, R. J. Good, *J. Phys. Chem.* **1957**, *61*, 904.

- [65] D. Cwikel, Q. Zhao, C. Liu, X. Su, A. Marmur, *Langmuir* **2010**, *26*, 15289.
- [66] A. Cassie, S. Baxter, *J. Chem. Soc., Faraday Trans.* **1944**, *40*, 546.
- [67] R. N. Wenzel, *Ind. Eng. Chem. Res.* **1936**, *28*, 988.
- [68] P. S. Brown, B. Bhushan, *Sci. Rep.* **2016**, *6*, 21048.
- [69] W. S. Y. Wong, A. Naga, L. Hauer, P. Baumli, H. Bauer, K. I. Hegner, M. D'Acunzi, A. Kaltbeitzel, H.-J. Butt, D. Vollmer, *Nat. Commun.* **2021**, *12*, 5358.
- [70] K. I. Hegner, W. S. Y. Wong, D. Vollmer, *Adv. Mater.* **2021**, *33*, 2101855.
- [71] M. K. C. Sridhar, C. R. Reddy, *Environ. Pollut. B* **1984**, *7*, 49.
- [72] P. Papadopoulos, L. Mammen, X. Deng, D. Vollmer, H.-J. Butt, *Proc. Natl. Acad. Sci. USA* **2013**, *110*, 3254.
- [73] P. Papadopoulos, D. Vollmer, H.-J. Butt, *Phys. Rev. Lett.* **2016**, *117*, 046102.
- [74] H. C. Hamaker, *Physica* **1937**, *4*, 1058.
- [75] R. Manica, E. Klaseboer, D. Y. C. Chan, *Adv. Colloid Interface Sci.* **2016**, *235*, 214.
- [76] D. Y. C. Chan, E. Klaseboer, R. Manica, *Soft Matter* **2011**, *7*, 2235.
- [77] C. Shi, X. Cui, X. Zhang, P. Tchoukov, Q. Liu, N. Encinas, M. Paven, F. Geyer, D. Vollmer, Z. Xu, H.-J. Butt, H. Zeng, *Langmuir* **2015**, *31*, 7317.